

# Ultrafast exciton relaxation in monolayer transition metal dichalcogenides

A. Thilagam\*

*Information Technology, Engineering and Environment,  
University of South Australia, Australia 5095.*

We examine a mechanism by which excitons undergo ultrafast relaxation in common monolayer transition metal dichalcogenides. It is shown that at densities  $\approx 1 \times 10^{11} \text{ cm}^{-2}$  and temperatures  $\leq 60 \text{ K}$ , excitons in well known monolayers ( $\text{MoS}_2$ ,  $\text{MoSe}_2$ ,  $\text{WS}_2$  and  $\text{WSe}_2$ ) exist as point-like structureless electron-hole quasiparticles. We evaluate the average rate of exciton energy relaxation due to acoustic phonons via the deformation potential and the piezoelectric coupling mechanisms and examine the effect of spreading of the excitonic wavefunction into the region perpendicular to the monolayer plane. Our results show that the exciton relaxation rate is enhanced with increase in the exciton temperature, while it is decreased with increase in the lattice temperature. Good agreements with available experimental data are obtained when the calculations are extrapolated to room temperatures. A unified approach taking into account the deformation potential and piezoelectric coupling mechanisms shows that exciton relaxation induced by phonons is as significant as defect assisted scattering and trapping of excitons by surface states in monolayer transition metal dichalcogenides.

## I. INTRODUCTION

In recent years, several works have examined the occurrences of large exciton binding energies<sup>1–6</sup> as well as exciton mediated ultrafast processes<sup>7–9</sup> that are enhanced in atomically thin layered transition metal dichalcogenides  $\text{MX}_2$  ( $\text{M} = \text{Mo}, \text{W}, \text{Nb}$ , and  $\text{X} = \text{S}, \text{Se}$ )<sup>10–12</sup>. The monolayer Molybdenum and Tungsten dichalcogenides ( $\text{MoS}_2$ ,  $\text{MoSe}_2$ ,  $\text{WS}_2$  and  $\text{WSe}_2$ ) generally have similar lattice parameters and electronic configurations<sup>13,14</sup>. Transition metal dichalcogenides are known to undergo a crossover from indirect band gap (bilayer) to direct gap in the monolayer configuration<sup>3</sup> where there is strong photoluminescence. The intrinsic band gap range from 0.5 eV to 2 eV, depending on the material composition and number of layers in the material system. Specifically, the confinement of charge carriers within a monolayer space results in an enhanced interaction of the exciton with light, a desirable property that can be exploited to fabricate highly sensitive photodetectors and sensor devices.

The study of exciton based quantum dynamical processes is important as excitonic interactions underlie the unique optoelectronic properties<sup>5,15–18</sup> of monolayer dichalcogenides. Several applications<sup>19–24</sup> can be linked to the rich many-body effects of excitons in low-dimensional transition metal dichalcogenides. The long lifetimes of excitons in transition metal dichalcogenides enable interaction with additional degrees of freedom linked to the unique optical selection rules of the momentum valleys<sup>25,26</sup> of two-dimensional  $\text{MX}_2$  materials. This enables tuning of the coupling strength of the valley to spin degrees of freedom, which results in desirable valleytronics properties<sup>27</sup> essential for high speed logic devices. A comprehensive understanding of the quantum dynamical processes of two-dimensional excitons is needed to fully exploit the unique properties of monolayer transition metal dichalcogenides for electrooptical and valleytronic devices.

Exciton dynamics in monolayer and few-layer  $\text{MoS}_2$  2D crystals examined using femtosecond transient absorption spectroscopy and microscopy techniques<sup>28</sup> show a highly enhanced intraband relaxation rate  $\leq 0.5 \text{ ps}$  in the monolayer configuration compared to 20 ps in the bulk material. This enhanced relaxation rate was attributed to increased defect assisted scattering and trapping of excitons by surface states<sup>28</sup>. The rapid capture rates of excitons by mid-gap defects from Auger processes was estimated to be about less than a picosecond to a few picoseconds in monolayer metal dichalcogenides<sup>29</sup>. The capture rates which display both linear and quadratic dependences on the exciton density arises primarily from the large overlap of the defect state wavefunction with the conduction or valence band Bloch state wavefunctions. The exciton capture rates are almost comparable to the exciton-exciton annihilation (EEA) rates<sup>8,30</sup> that becomes dominant as a result of the reduced Coulomb screening of spatially confined charge carriers in layered transition metal dichalcogenides.

The layered structures of metal chalcogenides give rise to a variety of phonon modes that interact via short range and long range forces with unique thickness dependences of phonons in layered transition metal dichalcogenides<sup>31–33</sup>. There exist two Raman active modes,  $A_{1g}$  and  $E_{2g}^1$  which exhibit frequency shifts with layer thickness in  $\text{MoS}_2$ <sup>31,32,34</sup>. The  $A_{1g}$  mode is associated with the out-of-plane displacement of S atoms while the  $E_{2g}^1$  is associated with the in-plane but opposing displacements of Mo and S atoms<sup>31,34</sup>. Photoluminescence studies of single-layer  $\text{MoS}_2$ <sup>35</sup> reveal a long-lived component due to exciton-phonon scattering, which highlights the importance of exciton interaction with phonons. The occurrence of interface and confined slab phonon modes<sup>36</sup> and dimensionality dependent exciton-phonon interactions in low-dimensional material systems<sup>37</sup> has not been fully examined in monolayer metal dichalcogenides. To this end, the possibility of an enhanced exciton relaxation arising from phonon assisted mechanism remains to be explored in few-layer transition metal dichalcogenide systems. In this study we consider the critical role played by phonons during exciton relaxation processes and compare computed rates of exciton energy relaxation with estimates of enhanced exciton relaxation rates associated with surface defects<sup>28,29</sup> in monolayer and few-layer samples.

In the monolayer transition-metal dichalcogenides, a direct band gap between the conduction and valence band extrema occurs

at the  $K$  point. While an energy minimum occurs at the  $Q$  point along the  $K - \Gamma$  axis at the lowest conduction band, energy is maximized at the  $\Gamma$  point of the valence band<sup>38</sup>. Charge carriers are generally located in the  $K, K'$  conduction band valleys which are approximately parabolic for energies less than 300 eV<sup>4</sup>. The direct excitonic transitions are enhanced at the two extremal locations of the  $K$  point in the monolayer configuration. Newly formed quasi-two-dimensional excitons that possess a finite center-of-mass motion momentum wave vector undergo one of four main processes : (1) jump to higher energy band states via absorption of phonons, (2) relax to lower kinetic energies via emission of phonons, (3) decay non-radiatively or radiatively to the continuum state and lastly (4) decay into free electron and holes that subsequently relax via phonon emission to lower energy levels.

In this study, we consider that newly formed electron-hole pairs lose energy via emission of longitudinal-acoustic (LA) and/or transverse-acoustic (TA) phonons via the deformation potential coupling channel. The exciton relaxation is initiated by deformations of the lattice potentials by acoustic phonons which is applicable at the low temperature range. The low dimensional excitons are considered to undergo further energy relaxation along the exciton dispersion curves before reaching a minimum in exciton energy. The temperature range of 5 – 70 K considered here therefore excludes the possibility of exciton relaxation via optical phonon modes as these transitions involve higher energies. Piezoelectricity which arises from the linear coupling between the electrical polarization and mechanical strain within a crystal have reasonable strengths in monolayer metal dichalcogenides<sup>39–42</sup>. The two-dimensional hexagonal crystal structure lacks an inversion symmetry, hence there occurs a strain field which gives rise to the piezoelectric properties in transition metal dichalcogenides. We therefore include the scattering of exciton due to the piezoelectric coupling via acoustic phonons in this study.

The paper is organized as follows. In Sec. II, we present the theoretical form of exciton wavefunction which is suitable for modeling the correlated electron-hole pair in monolayer transition metal dichalcogenides. In Sec. III, we discuss the Maxwell-Boltzmann and Bose-Einstein exciton distributions, and justify our choice of a suitable exciton distribution based on the material properties of the monolayer dichalcogenides given in Table-I. We also discuss the conditions required for a statistically degenerate system of excitons to occur in monolayer systems. In Sec. IV we present an explicit form of a quasi-two dimensional exciton-acoustic phonon interaction operator applicable in monolayer systems. This operator is used to derive the average rate of exciton energy relaxation,  $\langle \frac{dE}{dt} \rangle$  in Sec. V. Numerical results are presented for the monolayer transition metal dichalcogenides, MoS<sub>2</sub>, MoSe<sub>2</sub>, WS<sub>2</sub> and WSe<sub>2</sub> and differences in their relaxation properties are analyzed in Sec. V. The theory of exciton relaxation due to the piezoelectric coupling mechanism is presented in Sec. VI along with analysis of numerical results based on the piezoelectric properties of transition metal dichalcogenides. Lastly, conclusions are summarized in Sec. VII.

## II. EXCITON WAVEFUNCTION IN THE MONOLAYER TRANSITION METAL DICHALCOGENIDES

In transition metal dichalcogenides (MX<sub>2</sub>) the intra-layers of the M metal planes are held between the chalcogen X atomic planes by covalent bonding. The inter-layers can be easily separated into distinct layers<sup>43,44</sup> of just a few atomic layers. A hexagonally ordered plane of metal atoms sandwiched between two other hexagon planes of chalcogen atom represents a single monolayer which we examine using a quasi two-dimensional space. This is justified as the motion of the exciton is mostly confined within the parallel two-dimensional  $XY$  layers of the atomic planes and there is restricted exciton motion in the  $z$  direction perpendicular to the monolayer plane. Accordingly, the exciton is represented by a quasi-two dimensional wavefunction<sup>45</sup>, and for simplicity we introduce the two-band approximation involving the lowest electron subband and highest hole subband structure. The exciton state vector denoted by  $|\alpha, \mathbf{K}\rangle$  in the presence of phonons can then be written as

$$|\alpha = 1s, \mathbf{K}\rangle = \frac{v_o}{L} \sum_{\mathbf{r}_e, \mathbf{r}_h} \exp(i\mathbf{K} \cdot \mathbf{R}) \Psi_{1s}(\mathbf{r}_e - \mathbf{r}_h, z_e, z_h) a_{1, \mathbf{r}_e}^\dagger a_{0, \mathbf{r}_h} |0, n\rangle, \quad (1)$$

where  $v_o$  is the volume of the unit cell and  $L$  is a quantized length of the lattice space. We restrict this study to the the lowest 1s exciton state without great loss in generality. The co-ordinate of the centre of mass of an exciton,  $\mathbf{R}$  is given by

$$\mathbf{R} = \alpha_e \mathbf{r}_e + \alpha_h \mathbf{r}_h, \quad (2)$$

$$\alpha_e = \frac{m_h}{m_e + m_h}, \quad \alpha_h = \frac{m_e}{m_e + m_h}, \quad (3)$$

where  $m_e$  ( $m_h$ ) is the effective mass of the electron (hole). The position vectors and wave vectors are decomposed into components parallel and perpendicular to the monolayer plane as  $\mathbf{r} = (r_{\parallel}, z)$  and  $\mathbf{k} = (k_{\parallel}, k_z)$  respectively. The creation operator of an electron in the conduction band at position  $r_e$  is denoted by  $a_{1, \mathbf{r}_e}^\dagger$ . The annihilation operator of an electron in the valence band at position  $r_h$  is denoted by  $a_{0, \mathbf{r}_h}$ . The state  $|0, n\rangle$  in Eq.1 is given by

$$|0, n\rangle = |0\rangle |n\rangle \quad (4)$$

where  $|0\rangle$  is the electronic vacuum state of the system that represents completely filled valence bands and empty conduction bands. The occupation number of phonons with wavevector  $\mathbf{q}$  is given by

$$|n\rangle = |n_1, n_2, \dots, n_{\mathbf{q}}\rangle \quad (5)$$

In Eq.1,  $\Psi_{1s}(\mathbf{r}_e - \mathbf{r}_h, z_e, z_h)$  denotes the 1st state exciton envelope function in the in the monolayer configuration. This state has the variational envelope function which appear as<sup>46</sup>

$$\Psi_{1s}(\rho, z_e, z_h) = \mathcal{N} \exp \left[ -(\gamma^2 \rho^2 + \beta^2 (z_e - z_h)^2)^{1/2} \right] \cos\left[\frac{\pi z_e}{L_w}\right] \cos\left[\frac{\pi z_h}{L_w}\right], \quad (6)$$

where  $\mathcal{N}$  is the normalization constant and  $\rho = |\mathbf{r}_e - \mathbf{r}_h|$  is the relative separation of the electron-hole pair in the monolayer plane. We have assumed that the excitonic wavefunction undergoes a discontinuous transition to zero beyond the region  $|z_e| < \frac{L_w}{2}$  and  $|z_h| < \frac{L_w}{2}$ , where  $L_w$  is the average displacement of electrons and holes in the  $z$  direction, perpendicular to the monolayer surface. The parameters  $\beta$  and  $\gamma$  are determined by minimalizing the energy of the exciton in the presence of phonons, a task that is not numerically trivial. We therefore treat  $\beta$  and  $\gamma$  as adjustable parameters that appear as inverses of the confinement lengths parallel and perpendicular to the monolayer plane. For the exact two dimensional case,  $\beta L_w = 0$ .

We express the operators of Eq. (1) in the Bloch representation and convert the summation over  $\mathbf{r}_e$  and  $\mathbf{r}_h$  into integral form and obtain

$$|\alpha = 1s, \mathbf{K}\rangle = \sum_{\mathbf{k}, \mathbf{k}'} \Phi_{1s}(\mathbf{k}, \mathbf{k}', \mathbf{K}) \delta_{\mathbf{k}-\mathbf{k}', \mathbf{K}} a_{1, \mathbf{k}}^\dagger a_{0, \mathbf{k}'} |0, n\rangle \quad (7)$$

where  $\mathbf{k}$  and  $\mathbf{k}'$  are the wavevectors of electron and hole respectively and

$$\Phi_{1s}(\mathbf{k}, \mathbf{k}', \mathbf{K}) = \frac{1}{L^2} \int d^2r \int dz_e \int dz_h \Psi_{1s}(\mathbf{r}_e - \mathbf{r}_h, z_e, z_h) \exp[i(\alpha_e \mathbf{K} - \mathbf{k}) \cdot \mathbf{r} - i\mathbf{k}_z z_e + i\mathbf{k}'_z z_h], \quad (8)$$

where  $\alpha_e$  and  $\alpha_h$  are specified in Eq.3.

### III. MAXWELL-BOLTZMANN VERSUS BOSE-EINSTEIN EXCITON DISTRIBUTIONS

The results of exciton relaxation kinetics is very much dependent on the type of exciton distribution employed during the modeling process. A widely used distribution is the Maxwell-Boltzmann function which appear as

$$f_{mw}(E) = \exp(-k_b T_{ex}), \quad (9)$$

where  $T_{ex}$  denotes the exciton temperature and  $k_b$  is the boltzmann constant. The total number of excitons can be easily evaluated as

$$N = \sum_{\mathbf{K}_{\parallel}} f_b(E(\mathbf{K}_{\parallel})) = \frac{M k_b T_{ex} L^2}{2\pi \hbar^2}, \quad (10)$$

where  $L$  is the quantization length and  $M$  is the exciton mass. The distribution in Eq.10 is applicable to the classical model of quasi-equilibrium of low dimensional excitons. The Maxwell-Boltzmann statistical distribution of excitons is suited for the temperature range,  $T \gg T_0$  where the degeneracy temperature  $T_0$  is given by<sup>47</sup>

$$T_0 = \left( \frac{2\pi \hbar^2 n_{ex}}{g M k_b} \right), \quad (11)$$

where  $n_{ex}$  is the exciton density, and the degeneracy factor  $g = 4$ , expressed a product of the spin and valley degeneracy factors<sup>48</sup>.

The exciton distribution function based on the Bose-Einstein distribution is given by

$$f_b(E) = \left[ \exp\left(\frac{E - \mu_{ex}}{K_B T_{ex}}\right) - 1 \right]^{-1}, \quad (12)$$

$$\mu_{ex} = K_B T_{ex} \ln \left[ 1 - \exp\left(-\frac{2\pi \hbar^2 n_{ex}}{g M k_b T_{ex}}\right) \right], \quad (13)$$

where the quasi-two dimensional exciton chemical potential  $\mu_{ex}$  is dependent on the exciton temperature  $T_{ex}$  and exciton density  $n_{ex}$ <sup>47</sup>. We evaluate the total number of excitons as

$$\begin{aligned} N &= \sum_{\mathbf{K}_{\parallel}} f(E(\mathbf{K}_{\parallel})) \\ &= \frac{M k_b T_{ex} L^2}{\pi \hbar^2} \log[1 - \exp(-\frac{\mu_{ex}}{k_b T})] \end{aligned} \quad (14)$$

From Eq. 14, it is seen that the Bose-Einstein distribution of excitons is the most appropriate model at low temperatures for which there exist a large exciton population with small wavevectors.

In the case of MoS<sub>2</sub>, we substitute the exciton density,  $n_{ex} = 1 \times 10^{11} \text{ cm}^{-2}$ , and  $m_e = 0.51$ ,  $m_h = 0.58$ <sup>38</sup> in Eq.11 which gives  $T_0 = 1.3 \text{ K}$ . The exciton density of  $1 \times 10^{11} \text{ cm}^{-2}$  corresponds to an inter-particle distance of  $316 \text{ \AA}$ , which is about 35 times the size of the exciton radius of  $9 \text{ \AA}$ <sup>6</sup>. Thus at typical exciton temperatures greater than 10 K, the excitons in the MoS<sub>2</sub> monolayer can be considered as well-defined correlated electron-hole quasi-particles. Excitons can also be modeled as point-like structureless systems provided the exciton de Broglie wavelength ( $\lambda_{db} = \hbar/\sqrt{2mT}$ ) far exceeds the exciton Bohr radius  $a_B$ . Based on the material properties of the monolayer transition metal dichalcogenides, MoS<sub>2</sub>, MoSe<sub>2</sub>, WS<sub>2</sub> and WSe<sub>2</sub> (given in Table-I), the ratio  $\frac{a_B}{\lambda_{db}}$  is plotted as a function of the exciton temperature  $T_{ex}$  in Fig. 1a. There are subtle differences due to varying material properties of the four types of monolayer systems. In general, the Maxwellian distribution appears appropriate for comparatively low exciton temperatures,  $T_{ex} \leq 60 \text{ K}$  and moderate exciton densities,  $n_{ex} \approx 1 \times 10^{11} \text{ cm}^{-2}$  (see Fig. 1b). We therefore restrict  $T_{ex}$  to the classical temperature range and exciton concentration to examine the exciton relaxation pathways in this study.

In Fig. 1b, the degeneracy temperature  $T_0$  (Eq.11) is plotted as a function of the exciton density  $n_{ex}$ , for MoS<sub>2</sub>, MoSe<sub>2</sub>, WS<sub>2</sub> and WSe<sub>2</sub>. The  $m_e$  and  $m_h$  values used in the calculations are retrieved from Ref.<sup>38</sup> (see Table-I). Tungsten sulphide yields the highest estimate of  $T_0$  which can be partly attributed to its comparatively small exciton mass ( $m_e + m_h$ ). The sulfides possess a higher  $T_0$  than the selenides. The results in Fig. 1 show that at high enough exciton densities  $n_{ex} > 2 \times 10^{12} \text{ cm}^{-2}$ , there is possible occurrence of a statistically degenerate system of excitons. This gives rise to relaxation mechanisms that are dependent on the Bose-Einstein statistical distribution of the excitons. In this study, we choose a lower density  $n_{ex} = 1 \times 10^{11} \text{ cm}^{-2}$  so as to exclude degenerate effects.

Applying Eq.13 to the monolayer MoS<sub>2</sub>, we obtain the negative exciton chemical potential  $\mu_{ex} = -4.8 \text{ meV}$  at exciton temperature  $T_{ex} = 20 \text{ meV}$  and the density,  $n_{ex} = 1 \times 10^{11} \text{ cm}^{-2}$ . The chemical potential assumes negative values of magnitude larger than 5 meV for  $T_{ex} > 20 \text{ meV}$ , hence condensation processes can be excluded at typical operating conditions<sup>28,29</sup> in MoS<sub>2</sub>. In Fig. 1c, the absolute value of the exciton chemical potential,  $|\mu_{ex}|$  is plotted as a function of the exciton temperature with exciton density fixed at  $n_{ex} = 1.5 \times 10^{11} \text{ cm}^{-2}$  for all the dichalcogenides. Molybdenum selenide yields the highest estimate of  $|\mu_{ex}|$  due to its comparatively large exciton mass ( $m_e + m_h$ ). The selenides show slightly higher  $|\mu_{ex}|$  than the sulfides, while the Molybdenum dichalcogenides have higher  $|\mu_{ex}|$  than the Tungsten dichalcogenides.

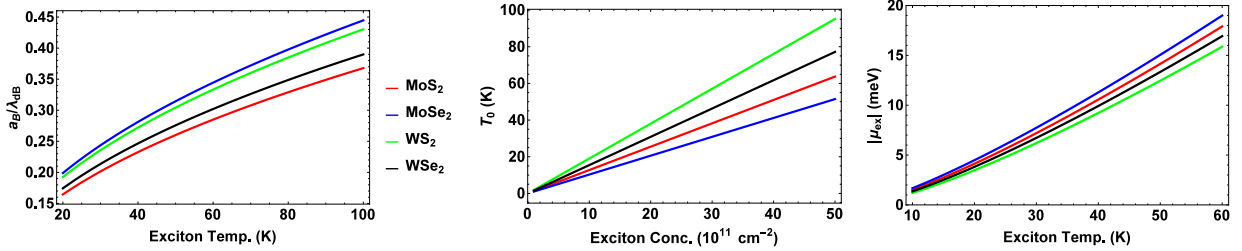


FIG. 1: (a) The ratio of exciton Bohr radius to the de Broglie wavelength ( $\frac{a_B}{\lambda_{db}}$ ) as a function of the exciton temperature  $T_{ex}$  for the four monolayer transition metal dichalcogenides, MoS<sub>2</sub>, MoSe<sub>2</sub>, WS<sub>2</sub> and WSe<sub>2</sub> (left), (b) The degeneracy temperature  $T_0$  (Eq.11) as a function of the exciton density  $n_{ex}$  (middle), (c) The absolute value of the exciton chemical potential,  $|\mu_{ex}|$  as a function of the exciton temperature, with the exciton density fixed at  $n_{ex} = 1.5 \times 10^{11} \text{ cm}^{-2}$  for all the dichalcogenides. (right).

#### IV. QUASI-TWO DIMENSIONAL EXCITON-ACOUSTIC PHONON INTERACTION OPERATOR

The three dimensional electron-phonon interaction due to the deformation-potential coupling can be written as

$$H_{e-ph}^{DF(3D)} = \sum_{\mathbf{k}, \mathbf{q}} \left( \frac{\hbar |\mathbf{q}|}{2\rho uV} \right)^{1/2} \left[ D_c a_{1, \mathbf{k}+\mathbf{q}}^\dagger a_{1, \mathbf{k}} + D_v a_{0, \mathbf{k}+\mathbf{q}}^\dagger a_{0, \mathbf{k}} \right] \times (b_{\mathbf{q}} + b_{-\mathbf{q}}^\dagger) \quad (15)$$

where  $D_c$  and  $D_v$  are the deformation potentials for the conduction and valence bands,  $\rho$  is the mass density of the bulk system and  $u$  is the sound velocity of the longitudinal-acoustic phonon mode in the material. The phonon creation and annihilation operators are indicated by  $b_{\mathbf{q}}^\dagger$  and  $b_{\mathbf{q}}$  respectively. An explicit form of the quasi-two dimensional operator can be obtained by projecting the matrix element of the three dimensional electron-phonon interaction operator between two quasi-two dimensional exciton states<sup>46</sup>. This approach assumes that the electron-hole internal motion remains unchanged during interaction with the phonons.

Using the wave function in Eq. (6), and the exciton state vector specified in Eqs. (7) and (8), the quasi-two dimensional exciton-phonon interaction operator can be obtained using Eq. (15)

$$H_{ex-ph}^{DF(Q2D)} = 4 \sum_{\mathbf{K}_{\parallel}, \mathbf{K}'_{\parallel}, q_z} \left( \frac{\hbar \sqrt{((\mathbf{K}_{\parallel} - \mathbf{K}'_{\parallel})^2 + q_z^2)}}{2 \varrho_m u_m S} \right)^{1/2} \left[ \frac{D_c \mathcal{W}(2\beta L_w, q_z L_w)}{[1 + (\lambda_h/2)^2]^{3/2}} - \frac{D_v \mathcal{W}(2\beta L_w, q_z L_w)}{[1 + (\lambda_e/2)^2]^{3/2}} \right] \times |1s, \mathbf{K}'_{\parallel}\rangle \langle \mathbf{K}_{\parallel}, 1s| (b_{\mathbf{K}'_{\parallel} - \mathbf{K}_{\parallel}, q_z} + b_{\mathbf{K}_{\parallel} - \mathbf{K}'_{\parallel}, q_z}^{\dagger}) \delta_{\mathbf{K} - \mathbf{K}', \mathbf{q}} \quad (16)$$

where  $\lambda_h = q\alpha_h/\gamma$  and  $\lambda_e = q\alpha_e/\gamma$ . The term  $S$  is the surface area of the monolayer plane,  $\varrho_m$  is the areal mass density and  $u_m$  is the sound velocity of the phonon mode in the monolayer system. The delta function in Eq. (16) conserves the momentum of the scattered exciton and phonon along the  $XY$  plane. The function  $\mathcal{W}(a, b)$  is given by<sup>46</sup>

$$G(a, b) = \int_{-1/2}^{1/2} dz_e \int_{-1/2}^{1/2} dz_h \exp(ibz_e - a|z_e - z_h|)(1 + a|z_e - z_h|) \cos^2(\pi z_e) \cos^2(\pi z_h) \quad (17)$$

The explicit form of the function  $\mathcal{W}(a, b)$  is lengthy and we therefore derive  $\mathcal{W}(a, b)$  at specific values of  $a, b$ . At the limits ( $b \rightarrow 0$ ) and ( $a \rightarrow 0$ ) the function  $\mathcal{W}(a, b)$  take simple forms

$$\mathcal{W}(a, b \rightarrow 0) = [3e^a a^7 + 28\pi^2 e^a a^5 + 16\pi^4 (a + (6a - 7)e^a + 7) a^2 + 64\pi^6 (a + (2a - 3)e^a + 3)] \times \frac{e^{-a}}{2a^2 (a^2 + 4\pi^2)^3} \quad (18)$$

$$\mathcal{W}(a \rightarrow 0, b) = \frac{2\pi^2 \sin(\frac{b}{2})}{b(4\pi^2 - b^2)} \quad (19)$$

The ideal two dimensional electron-phonon interaction for the deformation-potential coupling can be obtained using Eqs. 16, 18 and 19 as

$$H_{ex-ph}^{DF(2D)} = \sum_{\mathbf{K}_{\parallel}, \mathbf{K}'_{\parallel}} \left( \frac{\hbar \sqrt{((\mathbf{K}_{\parallel} - \mathbf{K}'_{\parallel})^2)}}{2 \varrho_m u_m S} \right)^{1/2} \left[ \frac{D_c}{[1 + (\lambda_h/2)^2]^{3/2}} - \frac{D_v}{[1 + (\lambda_e/2)^2]^{3/2}} \right] \times |1s, \mathbf{K}'_{\parallel}\rangle \langle \mathbf{K}_{\parallel}, 1s| (b_{\mathbf{q}} + b_{-\mathbf{q}}^{\dagger}) \delta_{\mathbf{K} - \mathbf{K}', \mathbf{q}} \quad (20)$$

## V. RELAXATION OF EXCITON KINETIC ENERGY

At low lattice temperatures ( $\leq 30$  K), the exciton relaxes by losing its kinetic energy along the dispersion energy curves coupled with the emission of acoustic phonons. The overall rate at which phonons are emitted is dependent on the energy exchanges between the exciton and phonon during the intra-valley relaxation process. The net increase in the number of acoustic phonons is based on the emission rate of phonons with wave vector  $\mathbf{q} = (\mathbf{q}_{\parallel}, q_z)$

$$\frac{dN_{\mathbf{q}}}{dt} = \frac{4\pi M}{\hbar^3} \sum_{\mathbf{K}_{\parallel}} \int_0^{\pi} \frac{|H_{ex-ph}^{DF(Q2D)}(\mathbf{q}_{\parallel}, q_z)|^2}{|\mathbf{K}_{\parallel} \cdot \mathbf{q}_{\parallel} \sin(\theta)|} \delta(\theta - \theta_0) [(1 + \bar{n}_q) f(\mathbf{K}_{\parallel} + \mathbf{q}_{\parallel}) - \bar{n}_q f(\mathbf{K}_{\parallel})] d\theta, \quad (21)$$

where the thermalized average occupation of phonons  $\bar{n}_q = [\exp(\frac{\hbar\omega(q)}{k_B T}) - 1]^{-1}$ , and  $\hbar\omega(q)$  is the energy of phonon with wavevector  $q$ . The term  $f(\mathbf{K}_{\parallel})$  denotes the distribution function associated with the exciton wave vector  $\mathbf{K}_{\parallel}$ . During exciton scattering, the energy conservation rule  $|\mathbf{K}_{\parallel}| \geq K_l$  is obeyed, where  $K_l = |\frac{2M\omega}{\hbar} - \mathbf{q}_{\parallel}|^2$ . The angle between the exciton wave vector  $\mathbf{K}_{\parallel}$  and  $\mathbf{q}_{\parallel}$  is denoted by  $\theta_0$ .

The relation in Eq. 22 can be further simplified by assuming the action of comparatively large phonon wave vectors such that  $\mathbf{q}_{\parallel} \gg q_m$  where  $q_m = 2Mu_m/\hbar$  to the following form

$$\frac{dN_{\mathbf{q}}}{dt} = \frac{M^{3/2} L^2}{\sqrt{2\pi} \hbar^4} \frac{|H_{ex-ph}^{DF(Q2D)}(\mathbf{q}_{\parallel}, q_z)|^2}{|\mathbf{q}_{\parallel}|} \int_{E_l}^{\infty} \frac{dE}{\sqrt{(E - E_l)}} [(1 + \bar{n}_q) f(E + \hbar\omega(q)) - \bar{n}_q f(E)], \quad (22)$$



where  $E_l = \frac{\hbar^2 q_{\parallel}^2}{8M}$ . Substituting Eqs.9 and 10 into Eq.22, we obtain an expression for the average rate of exciton energy relaxation

$$\left\langle \frac{dE}{dt} \right\rangle = -\frac{1}{N} \sum_{\mathbf{q}_{\parallel}, q_z} \hbar \omega(q) \frac{dN_{\mathbf{q}}}{dt} \quad (23)$$

$$= \frac{\sqrt{2\pi M}}{\sqrt{k_b T_{ex}} \hbar^2} \sum_{\mathbf{q}_{\parallel}, q_z} \hbar \omega(q) \frac{|H_{ex-ph}^{DF(Q2D)}(\mathbf{q}_{\parallel}, q_z)|^2}{|\mathbf{q}_{\parallel}|} \exp\left(-\frac{E_l}{K_b T_{ex}}\right) \left[ (1 + \bar{n}_q) \exp\left(-\frac{\hbar \omega(q)}{K_b T_{ex}}\right) - \bar{n}_q \right] \quad (24)$$

To obtain an explicit expression for the average rate of exciton energy relaxation in Eq.23, we employ the form of the quasi-two dimensional exciton-phonon interaction term in Eq.16

$$\left\langle \frac{dE}{dt} \right\rangle = -\frac{\sqrt{2\pi M}}{\pi^2 \sqrt{k_b T_{ex}} \varrho_m} \sum_{q_z} \int_{q_m}^{\infty} dq q^2 \exp\left(-\frac{E_l}{K_b T_{ex}}\right) \left[ (1 + \bar{n}_q) \exp\left(-\frac{\hbar \omega(q)}{K_b T_{ex}}\right) - \bar{n}_q \right] \quad (25)$$

$$\times \left[ \frac{D_c \mathcal{W}(2\beta L_w, q_z L_w)}{[1 + (\lambda_h/2)^2]^{3/2}} - \frac{D_v \mathcal{W}(2\beta L_w, q_z L_w)}{[1 + (\lambda_e/2)^2]^{3/2}} \right]^2 \quad (26)$$

where  $q_m = 2Mu_m/\hbar$ . To simplify the numerical evaluation of  $\left\langle \frac{dE}{dt} \right\rangle$ , we use  $q_z = \frac{\pi}{L_w}$ , which does not affect the order of magnitude of the energy relaxation rate. Using the explicit form for  $\mathcal{W}(a, 2\pi)$  derived using Eq.17, we numerically evaluate  $\left\langle \frac{dE}{dt} \right\rangle$  for the four monolayer transition metal dichalcogenides, MoS<sub>2</sub>, MoSe<sub>2</sub>, WS<sub>2</sub> and WSe<sub>2</sub> based on the material parameters provided in Table-I.

Fig. 2a shows the increase in  $\left\langle \frac{dE}{dt} \right\rangle$  with exciton temperature  $T_{ex}$  for various monolayer transition metal dichalcogenides at a given lattice temperature  $T_L = 5$  K and confinement parameter  $\beta L_w = 0.25$ . The energy relaxation rates for MoS<sub>2</sub> lies in the range  $10^8 - 10^9$  eV/s for exciton temperatures less than 60 K. The phonon induced relaxation rates when extrapolated to higher temperatures with assumption of the Maxwellian distribution for excitons, match the experimental estimates of about  $10^{12}$  eV/s observed at room temperatures. The experimental results were previously attributed to defects assisted intra-band scattering processes<sup>28</sup>. We point out that only the relaxation channel via LO-phonons has been included to evaluate the results in Fig. 2a. We expect the additional channels provided by TO-phonons, as well scattering via piezoelectric coupling (Section VI) to further enhance exciton relaxation rates in monolayer systems. The results in Fig. 2 highlight the critical role played by acoustic phonons in inducing exciton relaxation processes and imply that exciton-phonon interactions can become as strong as exciton-defect interactions under favourable conditions.

Fig. 2a shows that the Molybdenum dichalcogenides experience the fastest energy relaxation due to their high exciton effective masses, low mass densities and high deformation potential constants. Due to similar material properties, the estimated  $\left\langle \frac{dE}{dt} \right\rangle$  are approximately the same for MoS<sub>2</sub> and MoSe<sub>2</sub> monolayer systems. Fig. 2b displays the mean relaxation rate  $\left\langle \frac{dE}{dt} \right\rangle$  as function of the lattice temperature at the exciton temperature  $T_{ex} = 40$  K and  $\beta L_w = 0.25$ . The results indicate a decrease in the effectiveness of the exciton-acoustic phonon interaction channel as the lattice temperature is increased. The parameter  $2\beta L_w$  yields a measure of confinement of the charge carriers in the direction perpendicular to the monolayer plane. The decline in  $\left\langle \frac{dE}{dt} \right\rangle$  with increase in  $2\beta L_w$  in Fig. 2c shows that reduction in dimensionality enhances energy relaxation rates in monolayer systems.

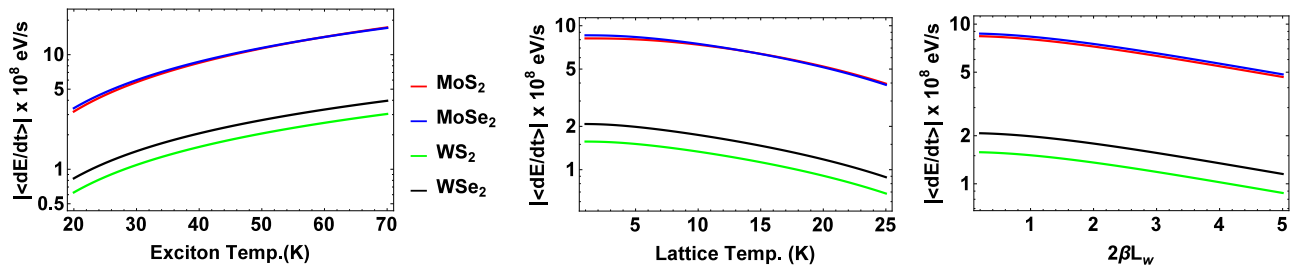


FIG. 2: (a) Mean relaxation rate  $\left\langle \frac{dE}{dt} \right\rangle$  as function of the exciton temperature  $T_{ex}$  in which the lattice temperature,  $T_L = 5$  K and  $\beta L_w = 0.25$  for monolayer transition metal dichalcogenides, MoS<sub>2</sub>, MoSe<sub>2</sub>, WS<sub>2</sub> and WSe<sub>2</sub>. (left), (b) Mean relaxation rate  $\left\langle \frac{dE}{dt} \right\rangle$  as function of the lattice temperature with exciton temperature  $T_{ex} = 40$  K and  $\beta L_w = 0.25$ , (c) Mean relaxation rate  $\left\langle \frac{dE}{dt} \right\rangle$  as function of parameter,  $2\beta L_w$  evaluated using exciton temperature  $T_{ex} = 35$  K and lattice temperature = 5 K (right)

## VI. EXCITON RELAXATION DUE TO THE PIEZOELECTRIC COUPLING MECHANISM

We express the piezoelectric exciton-phonon interaction operator in a form analogous to Eq.16 as

$$H_{ex-ph}^{DF(Q2D)} = \frac{4e}{\epsilon_0} \sum_{\mathbf{K}_{\parallel}, \mathbf{K}'_{\parallel}, q_z} \left( \frac{\hbar \sqrt{((\mathbf{K}_{\parallel} - \mathbf{K}'_{\parallel})^2 + q_z^2)}}{2\rho_m u_m S} \right)^{1/2} \left[ \frac{\mathbf{e}_{11} \mathcal{W}(\sqrt{4+\lambda_h^2} \beta L_w, q_z L_w)}{[1+(\lambda_h/2)^2]^{3/2}} - \frac{\mathbf{h}_{11} \mathcal{W}(\sqrt{4+\lambda_e^2} \beta L_w, q_z L_w)}{[1+(\lambda_e/2)^2]^{3/2}} \right] \times |1s, \mathbf{K}'_{\parallel}\rangle \langle \mathbf{K}_{\parallel}, 1s| (b_{\mathbf{K}'_{\parallel}-\mathbf{K}_{\parallel}, q_z} + b_{\mathbf{K}_{\parallel}-\mathbf{K}'_{\parallel}, q_z}^{\dagger}) \delta_{\mathbf{K}-\mathbf{K}', \mathbf{q}} \quad (27)$$

where  $\mathbf{e}_{11}$  ( $\mathbf{h}_{11}$ ) is the piezoelectric constant for the electron (hole), and  $\epsilon_0$  is the dielectric constant that is independent of the piezoelectric effect. As given in Eq.16,  $\rho_m$  is the areal mass density,  $u_m$  is the sound velocity of the phonon mode in the monolayer system and  $\lambda_h = q\alpha_h/\gamma$ ,  $\lambda_e = q\alpha_e/\gamma$ . Due to the coupling with the TA and LA phonons, piezoelectric interactions are anisotropic in nature. These anisotropic effects can be incorporated by considering the angular mean of the piezoelectric interaction, which introduces the factor  $\frac{1}{2}$  in Eq.27.

The piezoelectric constant has been estimated to be  $\mathbf{e}_{11} \approx 3 \times 10^{-11}$  C/m for monolayer  $\text{MoS}_2$ <sup>49</sup>, which is an order of magnitude less than the estimate  $3.64 \times 10^{-10}$  C/m provided by Duerloo et. al.<sup>50</sup> (Table-I). The reasons for the differences in the piezoelectric constant values for  $\text{MoS}_2$  from the two known sources<sup>49,50</sup> remain unresolved. According to the piezoelectric constants given in Ref.<sup>50</sup>, the Molybdenum dichalcogenides have higher piezoelectric strengths than the Tungsten dichalcogenides as can be seen in Table-I. So far all known piezoelectric constants<sup>49,50</sup> are linked to the linear coupling between the electrical polarization induced by the electron and strain field within the crystal. There is no mention of similar interactions associated with electrical polarization induced by the hole. In order to obtain numerical estimates of the exciton relaxation rates, we consider the difference  $|\mathbf{e}_{11} - \mathbf{h}_{11}| = \eta \times 10^{-10}$  C/m where the parameter  $\eta$  is varied from 0.1 to 1.5.

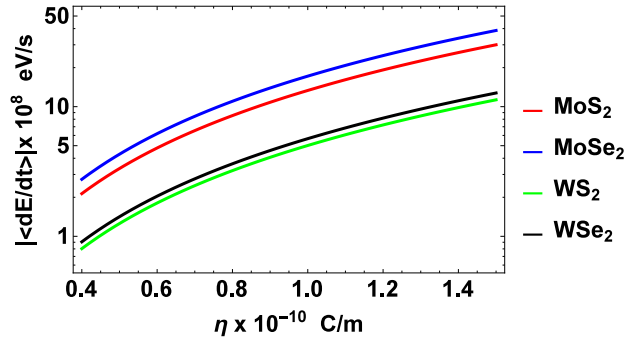


FIG. 3: Mean relaxation rate  $\langle \frac{dE}{dt} \rangle$  as function of the difference in piezoelectric constants  $|\mathbf{e}_{11} - \mathbf{h}_{11}| = \eta \times 10^{-10}$  C/m. The exciton temperature  $T_{ex} = 35$  K, and lattice temperature,  $T_L = 5$  K.

Using Eq.27 and the numerical scheme outlined in Section V, we evaluate the average rate of exciton energy relaxation  $\langle \frac{dE}{dt} \rangle$  as a function of the difference in piezoelectric constants,  $\eta \times 10^{-10}$  C/m. The results evaluated by setting exciton temperature  $T_{ex} = 35$  K, and lattice temperature,  $T_L = 5$  K are displayed in Fig. 3 for four monolayer transition metal dichalcogenides. In all materials, there is increase of  $\langle \frac{dE}{dt} \rangle$  with  $\eta$ , and values for  $\langle \frac{dE}{dt} \rangle$  lie in the range  $10^8 - 10^9$  eV/s for  $|\mathbf{e}_{11} - \mathbf{h}_{11}| \approx 10^{-10}$  C/m. The order of rates evaluated in Fig. 3 are comparable to results in Fig. 2 computed previously for exciton-phonon interaction due to the deformation potential mechanism. These results indicate that a unified approach for exciton-phonon interactions taking into account both deformation potential and piezoelectric mechanisms will yield a higher rate of exciton relaxation than those shown in Figs 2, 3. The results obtained in this study imply that exciton relaxation induced by phonons can become as important as defects assisted intra-band scattering processes<sup>28</sup>. The role of exciton-exciton interactions during energy relaxation has not been considered in this work. An earlier work<sup>51</sup> has shown that inter-excitonic interactions are sensitive to changes in the excitonic wavefunctions, indicating that such interactions may possibly be enhanced in monolayers compared to bulk systems. This can be attributed to the enhanced Coulomb coupling between electrons and holes. A detailed study of the role of inter-excitonic interactions on exciton-phonon interactions is beyond the scope of this work as this requires a refinement in the form of the variational envelope function employed in Eq.6. Nevertheless it would be worthwhile to examine whether exciton-exciton interactions will influence the phonon assisted exciton relaxation in future studies.

## VII. CONCLUSION

The confinement of excitons to a narrow region of space is an important property of monolayer structures that forms the basis for high excitonic binding energies and other desirable properties. In this work we have examined the relaxation of quasi-two dimensional excitons due to interactions with acoustic phonons via the deformation potential mechanism. The influence of piezoelectric coupling linked to electrostatic interaction between the acoustic phonons and the crystal polarisation field is also included in this study. The relaxation rates due to the corresponding scattering mechanisms are analyzed for common monolayer transition metal dichalcogenides ( $\text{MoS}_2$ ,  $\text{MoSe}_2$ ,  $\text{WS}_2$  and  $\text{WSe}_2$ ). The results obtained here indicate that exciton relaxation induced by phonons due to the deformation potential and piezoelectric coupling mechanisms are comparable to defects assisted intra-band scattering processes and trapping of excitons by surface states in monolayer transition metal dichalcogenides. The results also indicate that Molybdenum dichalcogenides undergo faster exciton energy relaxation than the Tungsten dichalcogenides.

The results obtained in this work have importance in the optimization of material properties for device applications and for further exploration of new ideas in physics for development of innovative optical and sensor devices. Future studies of the effects of phonons on the tunneling between valence and conduction band in a p-n junction<sup>54</sup> based on  $\text{MoS}_2$  monolayer systems are expected to provide useful results relevant for device operations. The electronic structures of transition metal dichalcogenides are complex and highly sensitive to electric and magnetic fields. To this end, further investigations on the maneuverability of the electronic structures and the influence of external fields on exciton-phonon interaction is expected to provide an improved understanding of the origins of desirable properties that can be exploited in the development of new devices for future industries.

---

\* thilaphys@gmail.com

- <sup>1</sup> M. M. Ugeda *et al.*, Nature materials **13**, 1091 (2014).
- <sup>2</sup> H. M. Hill *et al.*, Nano Letters **15**, 2992 (2015).
- <sup>3</sup> K. F. Mak, C. Lee, J. Hone, J. Shan, and T. F. Heinz, Physical Review Letters **105**, 136805 (2010).
- <sup>4</sup> T. Cheiwchanchamnangij and W. R. Lambrecht, Physical Review B **85**, 205302 (2012).
- <sup>5</sup> H.-P. Komsa and A. V. Krasheninnikov, Physical Review B **86**, 241201 (2012).
- <sup>6</sup> A. Thilagam, Journal of Applied Physics **116**, 053523 (2014).
- <sup>7</sup> E. M. Mannebach *et al.*, ACS Nano **8**, 10734 (2014).
- <sup>8</sup> S. Konabe and S. Okada, Physical Review B **90**, 155304 (2014).
- <sup>9</sup> H. Wang, C. Zhang, and F. Rana, Nano Letters **15**, 339 (2014).
- <sup>10</sup> J. Wilson and A. Yoffe, Advances in Physics **18**, 193 (1969).
- <sup>11</sup> Q. H. Wang, K. Kalantar-Zadeh, A. Kis, J. N. Coleman, and M. S. Strano, Nature Nanotechnology **7**, 699 (2012).
- <sup>12</sup> J. He, K. Hummer, and C. Franchini, Physical Review B **89**, 075409 (2014).
- <sup>13</sup> G.-B. Liu, D. Xiao, Y. Yao, X. Xu, and W. Yao, Chemical Society Reviews **44**, 2643 (2015).
- <sup>14</sup> J. Mann *et al.*, Advanced Materials **26**, 1399 (2014).
- <sup>15</sup> A. Kumar and P. Ahluwalia, Tunable electronic and dielectric properties of molybdenum disulfide, in  $\text{MoS}_2$ , pp. 53–76, Springer, 2014.
- <sup>16</sup> D. Y. Qiu, H. Felipe, and S. G. Louie, Physical Review letters **111**, 216805 (2013).
- <sup>17</sup> D. Jariwala, V. K. Sangwan, L. J. Lauhon, T. J. Marks, and M. C. Hersam, ACS Nano **8**, 1102 (2014).
- <sup>18</sup> D. Y. Qiu, T. Cao, and S. G. Louie, Physical Review Letters **115**, 176801 (2015).
- <sup>19</sup> D. Lembke, S. Bertolazzi, and A. Kis, Accounts of chemical research **48**, 100 (2015).
- <sup>20</sup> A. Pospischil, M. M. Furchi, and T. Mueller, Nature nanotechnology **9**, 257 (2014).
- <sup>21</sup> H. Zhang *et al.*, Optics express **22**, 7249 (2014).
- <sup>22</sup> M.-L. Tsai *et al.*, ACS Nano **8**, 8317 (2014).
- <sup>23</sup> B. Radisavljevic, M. B. Whitwick, and A. Kis, ACS Nano **5**, 9934 (2011).
- <sup>24</sup> Y. Yoon, K. Ganapathi, and S. Salahuddin, Nano Letters **11**, 3768 (2011).
- <sup>25</sup> D. Xiao, G.-B. Liu, W. Feng, X. Xu, and W. Yao, Physical Review Letters **108**, 196802 (2012).
- <sup>26</sup> R. Suzuki *et al.*, Nature nanotechnology **9**, 611 (2014).
- <sup>27</sup> C. Mai *et al.*, Nano Letters **14**, 202 (2013).
- <sup>28</sup> H. Shi *et al.*, ACS Nano **7**, 1072 (2013).
- <sup>29</sup> H. Wang *et al.*, Physical Review B **91**, 165411 (2015).
- <sup>30</sup> D. Sun *et al.*, Nano Letters **14**, 5625 (2014).
- <sup>31</sup> C. Lee *et al.*, ACS Nano **4**, 2695 (2010).
- <sup>32</sup> Y. Zhao *et al.*, Nano Letters **13**, 1007 (2013).
- <sup>33</sup> B. Chakraborty, H. Matte, A. Sood, and C. Rao, Journal of Raman Spectroscopy **44**, 92 (2013).
- <sup>34</sup> A. Molina-Sanchez and L. Wirtz, Physical Review B **84**, 155413 (2011).
- <sup>35</sup> T. Korn, S. Heydrich, M. Hirmer, J. Schmutzler, and C. Schüller, Applied Physics Letters **99**, 102109 (2011).
- <sup>36</sup> G. Hai, F. Peeters, and J. Devreese, Physical Review B **48**, 4666 (1993).
- <sup>37</sup> A. Thilagam, Physical Review B **56**, 9798 (1997).



- <sup>38</sup> Z. Jin, X. Li, J. T. Mullen, and K. W. Kim, Phys. Rev. B **90**, 045422 (2014).
- <sup>39</sup> M. M. Alyoruk, Y. Aierken, D. Cakır, F. M. Peeters, and C. Sevik, The Journal of Physical Chemistry C **119**, 23231 (2015).
- <sup>40</sup> H. Zhu, Y. Wang, J. Xiao, M. Liu, S. Xiong, Z. Wong, Z. Ye, Ziliang, Y. Ye, X. Yin, and X. Zhang, Xiang, Nature Nanotechnology **10**, 151 (2015).
- <sup>41</sup> K.-A. N. Duerloo, M. T. Ong, and E. J. Reed, Piezoelectricity in monolayers and bilayers of inorganic two-dimensional crystals, in *MRS Proceedings* Vol. 1556, pp. Mrss13–1556, Cambridge Univ Press, 2013.
- <sup>42</sup> E. J. Reed, Nature nanotechnology **10**, 106 (2015).
- <sup>43</sup> J. H. Cho *et al.*, Nature materials **7**, 900 (2008).
- <sup>44</sup> S. Mouri, Y. Miyauchi, and K. Matsuda, Nano Letters **13**, 5944 (2013).
- <sup>45</sup> A. Thilagam, Physica B: Condensed Matter **464**, 44 (2015).
- <sup>46</sup> T. Takagahara, Physical Review B **31**, 6552 (1985).
- <sup>47</sup> A. Ivanov, P. Littlewood, and H. Haug, Physical Review B **59**, 5032 (1999).
- <sup>48</sup> K. Kaasbjerg, K. S. Thygesen, and K. W. Jacobsen, Physical Review B **85**, 115317 (2012).
- <sup>49</sup> K. Kaasbjerg, K. S. Thygesen, and A.-P. Jauho, Physical Review B **87**, 235312 (2013).
- <sup>50</sup> K. Duerloo, M. Ong, and E. Reed. The Journal of Physical Chemistry Letters **3**, 2871 (2012).
- <sup>51</sup> A. Thilagam, Physical Review B **63**, 045321 (2001).
- <sup>52</sup> J. Kang, S. Tongay, J. Zhou, J. Li, and J. Wu, Applied Physics Letters **102**, 012111 (2013).
- <sup>53</sup> Y. Ding *et al.*, Physica B: Condensed Matter **406**, 2254 (2011).
- <sup>54</sup> P. Solomon *et al.*, Journal of Applied physics **95**, 5800 (2004).

TABLE I: Parameters used to obtain results for Fig.1, Fig.2 and Fig.3. The effective electron and hole masses,  $m_e^*, m_h^*$  (in terms of the free-electron mass) at the  $K$  energy valleys/peak are obtained from Ref.<sup>38</sup>. The lattice constant ( $a_s$  (Å)) result is read from Ref.<sup>52</sup> while the layer thickness  $h$  is taken from Ref.<sup>53</sup>. The deformation potential constants for electron- acoustic phonon (lowest conduction band) and hole-acoustic phonon interaction (highest valence band) associated with the carrier transition,  $K \rightarrow K$  are obtained from Ref.<sup>38</sup>. The sound velocities  $u_{LA}$  of the longitudinal acoustic phonon mode are derived from Ref.<sup>38</sup>. We evaluate the monolayer areal mass density using  $\varrho_m = \rho \times h$  where the bulk density  $\rho$  is retrieved using the ChemicalData database linked to the Mathematica software package. For the examined dichalcogenides, the bulk  $\rho = 5 \times 10^3$  kg/m<sup>3</sup> (MoS<sub>2</sub>),  $6 \times 10^3$  kg/m<sup>3</sup> (MoSe<sub>2</sub>),  $7.5 \times 10^3$  kg/m<sup>3</sup> (WSe<sub>2</sub>) and  $9.2 \times 10^3$  kg/m<sup>3</sup> (WS<sub>2</sub>). The estimated  $\varrho_m$  indicated in Table-1 show the same order of magnitude  $\rho \sim 10^{-7}$  g cm<sup>-2</sup> for all materials. The piezoelectric tensor coefficient  $e_{11}$  for the various monolayer dichalcogenide is taken from Ref.<sup>50</sup>. In the last two columns of Table-I, we evaluate the dimensionless quantity  $q_o = \frac{2Mu_m}{h} \times \frac{a_s}{2\pi}$  and the exciton bohr radius using  $a_B = 0.529 \frac{\epsilon}{\mu} \text{ Å}$  where  $\mu$  is the exciton reduced mass with  $\mu^{-1} = m_e^{-1} + m_h^{-1}$ . The effective dielectric constant  $\epsilon$  for each material is based on the estimates used in Ref.<sup>6</sup>.

System	$m_e, m_h$	$a_s$ (Å)	$h$ (Å)	$D_c^{op}$ (eV)	$D_v^{op}$ (eV)	$u_{LA} \times 10^5$ cm/s	$\varrho_m \times 10^{-7}$ g/cm <sup>2</sup>	$e_{11} \times 10^{-10}$ C/m	$q_o$	$a_B$ Å
MoS <sub>2</sub>	0.51, 0.58	3.18	3.13	4.5	2.5	6.6	1.56	3.64	0.006	7.5
MoSe <sub>2</sub>	0.64, 0.71	3.32	3.35	3.4	2.8	4.1	2.01	3.92	0.005	8.0
WS <sub>2</sub>	0.31, 0.42	3.18	3.14	3.2	1.7	4.3	2.36	2.71	0.003	10.6
WSe <sub>2</sub>	0.39, 0.51	3.32	3.36	3.2	2.1	3.3	3.09	2.47	0.003	8.6